Analysis of neutral particles in LMD-U

Sawanaga, Yuji
Interdisciplinary Graduate School of Engineering Sciences, Kyushu University

Itoh, Sanae-I.
Research Institute for Applied Mechanics, Kyushu University

Inagaki, Shigeru
Research Institute for Applied Mechanics, Kyushu University

Yagi, Masatoshi
Research Institute for Applied Mechanics, Kyushu University

https://doi.org/10.15017/27058

出版情報：九州大学応用力学研究所所報. 137, pp.101-115, 2009-09. Research Institute for Applied Mechanics, Kyushu University
バージョン：
権利関係：

Analysis of neutral particles in LMD-U

Yuji SAWANAGA*1, Sanae-I. ITOH*2, Shigeru INAGAKI*2 and Masatoshi YAGI*2
E-mail of corresponding author: *sawa@riam.kyushu-u.ac.jp*

(Received June 1, 2009)

Abstract

To clarify the effect of turbulent flow structure on the neutral particle, the neutral particle distribution of LMD-U is evaluated by using Monte Carlo code. The simulation resutls are compared with the neural particle pressure obtained by experiments.

Key words : *turbulent flow structure, neutral particle, LMD-U, Monte Carlo code*

1. Introduction

In today's world, our life strongly depends on consumption of energy. In 2005, total worldwise energy consumption was 5×10^{20} J with 86.5% derived from the combustion of fossil fuels. Since amount of fossil fuels on our earth are limited and they cause global warming, we should develop a new energy which is ecologically acceptable. Nuclear fusion is one of the most promising candidates for new energy resources. Nuclear fusion is the energy source of the sun and stars. On earth, fusion research is aimed at demonstrating that this energy source can be used to produce electricity in a safe and environmentally benign way. Magnetic confinement fusion is one of the approach to generating fusion energy that uses magnetic fields to confine the fusion fuel in the form of a plasma. There remains many issues to be resolved for the development of fusion reactor.

Turbulent transport in plasmas is one of the key issues to be clarified in fusion research, thus has been investigated extensively[1-4]. It is known that the various scale fluctuations interact each other and generate the various scale structures in turbulent plasma. The Large Mirror Device Upgrade (LMD-U) is developed in Kyushu University to study structure formation and selection rules in turbulent plasma. Neutral particles are one of the important parameters to control the turbulent state of low temperature LMD-U plasmas. Neutrals contribute to plasma density and destabilize drift waves by impeding charge neutralization through ion-electron and neutral-electron collisions. On the other hand, neutrals stabilize drift waves through ion-neutral collisions. Thus, the drift wave turbulence is influenced by neutrals. In fact, nonlinear dependence of turbulence state on neutral pressure (i.e. transition of turbulent state) is observed in the LMD-U. Moreover, analysis by numerical code named numerical linear device (NLD) predicts that neutrals play a key role to control turbulence structure. The turbulent structures of zonal-flows and streamers are predicted by NLD and in particular, streamer is observed under the low neutral pressure operation in LMD-U. Hence clarification of role of neutrals in LMD-U is important to understand the turbulent structure (including zonal-flows and streamers) formation mechanisms. In this thesis, we calculate neutral pressure in LMD-U using Monte carlo code and compared with experimental data to validate simulation model.

This thesis is organized as follows. In chapter 2, drift waves, zonal flow and roles of neutral particles on plasma turbulence are reviewed. The LMD-U device are also introduced. Chapter 3 is devoted to neutral pressure simulation. Model equation is introduced and simulation results are shown. In chapter 4, comparisons between simulation result and experimental observation in LMD-U are performed. In chapter 5, summary is given.

2. Review

The drift wave turbulence is considered to play an important role on the turbulent transport in magnetized plasmas. Recent works on theory have indicated the impact of zonal flows on the drift wave turbulence and the zonal flow has been observed in many devices. The drift wave instability and zonal flow formation are universal

*1 Interdisciplinary Graduate School of Engineering Sciences, Kyushu University
*2 Research Institute for Applied Mechanics, Kyushu University

physics. In this section, thus, we explain drift-wave instabilities and zonal flow, as typical example of structure formation through non-linear coupling of drift waves in turbulent plasmas. Another important keyword in this work is neutral particles. Any plasma in experimental device is affected by neutrals. The basic role of neutrals in plasma is also explained in this section.

2.1 Drift Waves

Even when there is no obvious driving force such as an electric or a gravitational field, a plasma is not in the perfect thermodynamic equilibrium as long as it is confined [5]. The plasma pressure tends to make the plasma expand, and the expansion energy can drive an instability. This type of free energy is always present in any confined plasma, and the resulting waves are called "universal instabilities".

The drift wave is a low frequency wave ($\omega \ll \Omega_{ci}$: ion cyclotron frequency) that is driven by pressure gradient ∇p of plasma [6]. When the plasma presides in limited area, the boundary of n_e=0 (n_e: plasma density) exists, then, a pressure gradient exists. Thus, it is possible that the drift wave always exists in bounded magnetized plasma and is one of the universal instabilities.

Drift waves have a small but finite component of wave number, k along magnetic field, B_0. The shape of constant density surfaces, resembles to the flute with a slight helical twist (Fig. 1). If we enlarge the cross section enclosed by the box in Fig . 1 and straighten it out into Cartesian geometry, it would be seen as in Fig. 2. The only driving force for the instability is the pressure gradient $k_B T \nabla n_0$ (k_B:Boltzmann constant, T: temperature, n_0: zeroth-order density), here we assume $k_B T$ = constant, for simplicity. If there is no zeroth-order electric field, the zeroth-order drifts are written by

$$\mathbf{v}_{i0} = \mathbf{v}_{Di} = \frac{k_B T_i}{eB_0}\frac{n_0'}{n_0}\hat{\mathbf{y}},$$

$$\mathbf{v}_{e0} = \mathbf{v}_{De} = -\frac{k_B T_e}{eB_0}\frac{n_0'}{n_0}\hat{\mathbf{y}},$$

and drift waves have a phase velocity of the order of v_{Di} or v_{De}, here $n' = \frac{\partial n_0}{\partial y}$. We shall show that ω/k_y is approximately equal to v_{De}.

Since drift waves have finite $k_\parallel$, electrons can flow along $\mathbf{B}_0$ to establish a thermodynamic equilibrium among themselves. They will then obey the Boltzmann relation

$$n_1/n_0 = e\phi_1/k_B T_e, \tag{2.1}$$

where n_1 is the first-order density, ϕ_1 is the first-order electrostatic potential. At point **A** in Fig. 2 the density is larger than in equilibrium, namely n_1 is positive , and therefore ϕ_1 is positive. Similarly, at point B, n_1 and

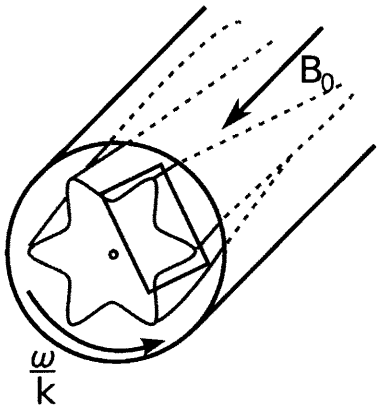

Fig. 1 Geometry of a drift instability in a cylinder. The region in the rectangle is shown in detail in Fig. 2.

ϕ_1 are negative. The difference in potential means there is an electric field $\mathbf{E}_1$ between A and B. The $\mathbf{E}_1$ causes the drift $\mathbf{v}_1 = \mathbf{E}_1 \times \mathbf{B}_o/B_0^2$ in the x direction. As the wave passes by, traveling in the y direction, an observer at point A will see n_1 and ϕ_1 oscillating in time. The drift $\mathbf{v}_1$ will also oscillate. Since there is a ∇n_0 in the x-direction, the drift $\mathbf{v}_1$ will bring plasma of different density to a fixed observer at point A. A drift wave, therefore, has a motion such that the fluid moves back and forth in the x-direction although the wave travels in the y-direction.

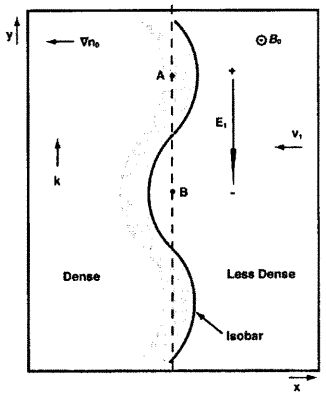

Fig. 2 Physical mechanism of a drift wave

To be more quantitative, the magnitude of v_{1x} is given by

$$v_{1x} = E_y/B_0 = -ik_y\phi_1/B_0. \tag{2.2}$$

We shall assume v_{1x} does not vary with x and that $k_\parallel$ is much smaller than k_y; that is, the fluid oscillates incompressibly in the x direction. Consider now the number of guiding centers brought at a fixed point A; it is obviously

$$\partial n_1/\partial t = -v_{1x}\partial n_0/\partial x. \tag{2.3}$$

This is just the equation of continuity for guiding centers, which, of course, do not have the fluid drift $\mathbf{v}_D$. The term $n_0\nabla\cdot\mathbf{v}_1$ vanishes because of our previous assumption of incompressibility. The difference between the density of guiding centers and the density of particles n_1 gives a correction to Eq.(2.3) which is higher order and may be neglected here. Using Eqs.(2.2) and (2.1), we can write Eq.(2.3) as

$$-i\omega n_1 = \frac{ik_y\phi_1}{B_0}n_0' = -i\omega\frac{e\phi_1}{k_B T_e}n_0,$$

Thus we have

$$\frac{\omega}{k_y} = -\frac{k_B T_e}{eB_0}\frac{n_0'}{n_0} = v_{De}.$$

These waves, therefore, travel with the velocity in the y (or azimuthal) direction. In addition, they must satisfy the conditions

$$k_\parallel \ll k_y \qquad v_{thi} \ll \omega/k_\parallel \ll v_{the}$$

where v_{thi} is ion thermal velocity and v_{the} is electron thermal velocity.

To see why drift waves are unstable, one must realize that v_{1x} is not quite E_y/B_0 for the ions. There are corrections due to the polarization drift and the non-uniform $\mathbf{E}$ drift. The result of these drifts is always to make the potential distribution ϕ_1 phase lag behind the density distribution n_1. This phase shift causes $\mathbf{v}_1$ to be outward where the plasma has already been shifted outward, and vice versa, hence the perturbation grows. When the resistivity comes in, the field $\mathbf{E}_1$ is not be short-circuited by electron flow along $\mathbf{B}_0$. Electron-ion collisions, together with a long distance $\frac{1}{2}\lambda_z$ (λ: mean free path) between crest and trough of the wave, make it possible to have a resistive potential drop and a finite value of $\mathbf{E}_1$. The dispersion relation for resistive drift waves is approximately given by

$$\omega^2 + i\sigma_\parallel(\omega-\omega_*) = 0\,, \qquad (2.4\text{ a})$$

$$\sigma_\parallel \equiv \frac{k_\parallel^2}{k_y^2}\Omega_{ci}(\Omega_{ce}\tau_{ei})\,, \qquad (2.4\text{ b})$$

where $\omega_* \equiv k_y v_{De}$, Ω_{ci} is ion cyclotron frequency and $\sigma_\parallel$ is the parallel conductivity.
If $\sigma_\parallel$ is large compared with ω, Eq.(2.4 a) can be satisfied only if $\omega \approx \omega_*$. In that case, we may replace ω by ω_* in the first term. Solving for ω, we then obtain

$$\omega \approx \omega_* + (i\omega_*^2/\sigma_\parallel)\,,$$

where $\omega_* = k_\perp T/BL_n$. This shows that $\mathrm{Im}(\omega)$ is always positive and is proportional to the resistivity $\eta = 1/\sigma_\parallel$. Drift waves are unstable and will eventually occur in any plasma with a density gradient. Fortunately, the growth rate is rather small, and there are ways to stabilize it by making $\mathbf{B}_0$ be shaped.

2.2 Zonal Flow

Zonal flows are low frequency, azimuthal symmetric band-like sheared flows (potential perturbations) with small radial scale [7,8]. Because of the importance of shared flows to the reduction of the turbulent transport, the importance of zonal flows is now well and widely appreciated. Zonal flows are intrinsically incapable of driving transport, and thus represent a reservoir of benign fluctuation energy. Zonal flows are non-lineary generated by drift waves via modulations of the radial flux of vorticity (i.e. charge separation current) and are damped by ion-ion collisions, by non-linear feedback on the underlying drift waves or (possibly) by Kelvin-Helmholtz type instabilities which disrupt them. In this manner Zonal flows are generated by drift waves and also damped by drift waves, and thus the drift wave-zonal flow co-exist system saturates. A predator-prey approach model indicates that multiple saturated states are possible. For the case of zonal flows, the methodology indicated in above section is not applicable since zonal flow field is stochastic and spatially complex. The mean shear decorrelation should be replaced by the random shear decorrelation due to zonal flows.

2.2.1 Suppression of Turbulent Transport

Mean shear flow and zonal flow can reduce or quench transport by altering either the turbulent fluctuations amplitude or the wave-particle correlation time, which determines the 'cross-phase' between, say $\tilde{V}_r$ and $\tilde{n}$, in the particle flux $\Gamma_r = \langle\tilde{n}\tilde{V}_r\rangle$. Up till now, we have been primarily concerned with effects on the fluctuation intensity. However, both zonal and mean shears can alter the correlation times and thus fluxes, even at fixed fluctuation amplitude.

The average cross-field flux is given in terms of cross correlations between various fluctuation fields. For instance, the radial particle flux is given by: $\Gamma_r = (1/B)\langle\tilde{n}\tilde{E}_\theta\rangle$. This flux, an averaged quantity, is determined by the amplitudes of density and electric field, and by the phase between them. In the case of electrostatic fluctuations, Γ_r can be written as:

$$\Gamma_r = \frac{1}{B}|\tilde{n}||\tilde{E}_\theta|\sin\alpha \qquad (2.5)$$

where α is the phase difference between the density and potential fluctutions. The α is determined by the wave-particle correlation time and by the response function. Obviously, shifting α can reduce (or increase) the flux. Here, we investigate the effect of mean shear on transport by analysing the response of a passive, phase-space field f (i.e. a distribution function) to a given ensemble of turbulence. A model equation for the passive advec-

tion of f in the presence of prescribed fluctuating $\tilde{v}$ (i.e. advecting velocity field) is:

$$\frac{\partial f}{\partial t} + v_{\parallel}\hat{b}\cdot\nabla f + \langle \boldsymbol{V}\rangle\cdot\nabla f + \tilde{v}\cdot\nabla f - D_c\nabla^2 f = 0 \ . \quad (2.6)$$

Here $\langle \boldsymbol{V}\rangle = V_y(x)\hat{y}$ is the mean sheared $\boldsymbol{E}\times\boldsymbol{B}$ flow, $b_{\parallel}^{i}$ is the parallel phase-space velocity and D_c is the collisional diffusion coefficient. We focus on strong turbulence, and consider the asymptotic limit where $D_c \to 0$. A formal solution for the cross field flux, $\Gamma_f \equiv \langle \tilde{f}^* \tilde{v_x}\rangle$ ($\langle\rangle$ is a flux surface average), is then given by

$$\Gamma_f = Re\sum_{k,\omega} \frac{i|x,\tilde{k},\omega|^2}{\omega - k_{\parallel}v_{\parallel} - k_y x S_v + i\tau_{ck}^{-1}} \frac{d}{dx} f_0 \ . \quad (2.7)$$

Note that equation (2.7) contains many time scales for irreversible dynamics, which must be considered. These are:

(a)$\Delta\omega_k$–the mode self-correlation decay rate, or inverse lifetime, due to nonlinear scrambling;

(b)Doppler spread (autocorrelation) rates:

$|k\Delta(\omega/k)|$–the spectral self-spreading (autocorrelation) rate, i.e. the inverse; lifetime of the spectral pattern (reflects the effect of dispersion–linear process);

$|k_{\parallel}v_{\parallel}\Delta x|$–the parallel Doppler spread (autocorrelation) rate, i.e. the rate at which parallel Doppler shift $k_{\parallel}v_{\parallel}$ changes with radius;

$|k_y S_v \Delta x|$–the shearing Doppler spread (autocorrelation) rate, i.e. the rate at which the sheared $\boldsymbol{E}\times\boldsymbol{B}$ flow-induced Doppler shift $k_y V_{\boldsymbol{E}\times\boldsymbol{B}}$ changes with radius;

(c)Decorrelation rates

$k_x^2 D_x$–particle decorrelation rate for radial scattering;

$(k_y^2 D_x S_v^2)^{1/3}$–particle decorrelation rate for hybrid of radial scattering in sheared flow, i.e. due to random walk in shearing coordinates;

$(k_{\parallel}'^2 v_{\parallel}^2 D_x)^{1/3}$– particle decorrelation rate for radial scattering in a sheared magnetic field.

Here Δx is the radial spectral width, D_x is the radial test diffusion coefficient, $k_{\parallel}' = k_{\parallel}/L_S$ and L_S is the shear length. Hereafter, parallel dynamics are ignored. Shearing becomes important when

$$|k_y S_v \Delta x| \gg k_x^2 D_x \sim \frac{D_x}{\Delta x^2}, |k_y S_v \Delta x| \gg \Delta\omega_k \ . \quad (2.8)$$

In this case, the relevant decorrelation rate is set by

$$\frac{1}{\tau_{ck}} = (k_y^2 D_y S_v^2)^{1/3} \ . \quad (2.9)$$

For $|k_y S_v \Delta x| \gg k_{\parallel}v_{\parallel}$, $|k_y S_v \Delta x|$ or $|\Delta k d\omega_k/dk|$ greater than $\Delta\omega_k$ and τ_{ck}^{-1}, Γ_j, can be simplified to $\Gamma_f \cong -\pi\Sigma_{k,\omega}|v_{x,k}^{\sim}|^2\delta(\omega_k - k_y S_v x)df_0/dx$. (An analytic expression $(\omega - k_y x S_v + ik_y^2 D_y)^{-1} \simeq -\pi\delta(\omega - k_y x S_v)$ is used.)The cross-field flux then reduces to:

$$\Gamma_f \cong -\pi \iint dm d\omega R|\frac{k_y}{L_S}|\frac{|\tilde{v}_{x,k}|^2}{|k_y S_v|}\frac{d}{dx}f_0 \quad (2.10)$$

Note that the flux depends on the spectral intensity at the resonance point $x_r = \omega/k_y S_v$. The assumption that this point falls within the spectral envelope is valid if $x_r < \Delta x$ or equivalently, $\omega < |k_x S_v \Delta x|$. Since we are concerned with the regimes of strong shear, this is almost always the case. In such strong shear regimes, then Γ_f scales inversely with S_v i.e.

$$\Gamma_f \propto S_v^{-1} \ . \quad (2.11)$$

A detailed analysis established that the passive scalar amplitude perturbation scales as $\sqrt{\langle(\tilde{f}/f/)^2\rangle} \propto S_v^{-5/6}$, so that

$$\sin\alpha \propto S_v^{-1/6} \ . \quad (2.12)$$

Note that the effect of even strong shear on the flux is modest ($\sim S_v^{-1}$) and its impact on the cross-phase is quite weak ($\sim S_v^{-1/6}$). Thus, the theory predicts that suppression of the cross-phase is weaker than reduction in turbulence intensity.

It is interesting to examine the scaling of D_x in the strong turbulence regime, for weak and strong shear. Noting that $\Gamma_f = -D_x(d/dx)f_0$, we have already established that $D_x \sim S_v^{-1}$ for strong shear and weak turbulence. In the case of strong shear and strong turbulence, $\tau_{ck}^{-1} > |k_y S_v \Delta x|$, so Γ_f is given by (from equation (2.7)): $\Gamma_f = -\mathrm{Re}\Sigma_{k,\omega}\tau_{ck}|v_{x,\tilde{k},\omega}|^2(d/dx)f_0$ i.e. $D_x = \tau_{ck}\langle\tilde{v}^2$. Taking equation (2.9) with $D_x \simeq D_y$ then gives

$$D_x \sim \frac{\langle\tilde{v}^2\rangle^{3/4}}{(k_y S_v)^{1/2}} \ , \quad (2.13)$$

which is consistent with the expected scaling $D_x \sim \omega_b(\Delta x_T)^2$ where ω_b is the particle bounce time in a poloidal wavelength, and Δx_T is the resonance width in radii.

Next, for the strong turbulence, weak shear case $1/\tau_{ck} = k_x^2 D_x$, so $D_x \sim \langle\tilde{v}^2\rangle^{1/2}(k_x^2)^{-1/2}$, which is the familiar scaling for transport in strong two-dimensional turbulence, first derived by Taylor and McNamara. Finally, we also note that the regime of strong shear (i.e. $|k_y S_v \Delta x| > \tau_{ck}^{-1}, \Delta\omega_k, \omega$) but with non-resonant response has also been investigated. The predictions are $\Gamma_f \sim S_v^{-2}$ and $\sin\alpha \propto S_v^{-2}$. The importance of this regime is dubious, though, since strong shear naturally favours a large shearing Doppler spread which in turn suggests the applicability of standard quasilinear theory and the occurrence of a resonant interaction.

In the previous subsection, we considered the effect of a mean shear flow on passive scalar flux and cross-phase. While understanding the case of a mean shear is necessary, it is certainly not sufficient for an understanding of the effects of a spectrum of zonal flows upon transport. Two additional features must be considered in the case

of zonal flows. These are:
(a) the flow pattern has a finite lifetime or self-correlation time, $\tau_{c,ZF}$;
(b) shearing occurs as a spectrum of scales, each corresponding to a radial zonal flow wavenumber q_r. The shearing pattern may be spatially complex.
The implication of differences (a) and (b) are that the effectiveness of shearing will be reduced (relative to that for equal strength mean flow) for short $\tau_{c,ZF}$, and that one should expect to find $S_{v,rms}$ (the rms value) replacing S_v n the quasilinear predictions given above, when $\tau_{c,ZF} \rightarrow \infty$. The details of these calculations have quite recently appeared in the literature.

2.3 Role of Neutral Particles in Plasma

2.3.1 Collision

In a plasma, collisions between the different kinds of particles play an important role since they can change the momentum and energy of the interacting particles [6]. Even more fundamental particle properties can be changed. For instance, the loss of electric charge in the case of ionization of an atom. Collision frequencies also dictate the dynamics of the drift mode, therefore numerical values of the collision frequencies are needed. Unfortunately, collision frequencies are difficult to determine accurately.
Besides elastic collisions, for collisions between ions and neutrals, the ion-atom charge transfer reaction $A + A^+ \rightarrow A^+ + A$ is also an important process. It can be seen that cross-sections for both processes are of the same order of magnitude and increase towards low energies where not much data exists. A formula for the cross-section for resonant charge exchange between an argon ion an argon atom(both in the ground state) is given:

$$\sigma_{in}[m^2] = 4.8 \times 10^{-19}(1 + 0.14\log(\frac{1[\mathrm{eV}]}{\mathrm{E[eV]}}))^2 \ . \quad (2.14)$$

Where E is the kinetic energy of the ion with respect to the atom. For the room temperature E=0.025eV, this yields $\sigma_{in} = 1.1 \times 10^{-18}m^2$. This is also in good agreement with the value of the total ion-atom cross-section at low temperatures of $\sim 10^{-18}m^2$. Ionization due to ion-atom collisions is significant only for energyies higher than 100eV and can therefore be neglected when discussing laboratory plasmas.

2.3.2 Reynolds Number

Reynolds number ($R \equiv vL/\nu$) of plasma is an important parameter for the excitation of the drift wave turbulence. Where, v is a fluid velocity, L is a typical scale length, ν is a viscosity. The viscosity of plasma results from the collisional effect. By using mean-free path, l, and collision time, τ, it can be written as

$$\nu \approx \frac{l^2}{\tau} \quad (2.14)$$

A large Reynolds number (i.e. small viscosity) is effective for exciting the turbulence. The viscosity in LMD-U plasma is controlled by varying of τ and l through adjusting neutral gas pressure and the magnetic field strength.

2.4 Large Mirror Device-Upgrade

The drift wave excitation experiments were performed in the Large Mirror Device Upgrade (LMD-U) [9-11]. The conception of the LMD-U aims at a flexible and versatile linear, magnetized plasma device that allows for various experiments on the dynamics of plasma waves and instabilities. A schematic view of the LMD-U is given in Figure 3.

The LMD-U is made by a stainless chamber with diameter of about 445 mm and axial length of 3740 mm. The coil system in the LMD-U produces a linear magnetic field configuration. A cylindrical helicon plasma with diameter of approximately 100 mm and axial length of 3740 mm is produced by a RF heating system (with a frequency 7MHz and the power of 3kW) and radially confined by the magnetic field. The typical operational condition and plasma parameters are shown in Fig 4. Langmuir probe systems are used to determine plasma parameters and observe density and potential fluctuations. A continuous argon gas is injected from the end of the RF system by a mass flow controller. Four turbo-molecular pumps and two buffle plates are installed to control the neutral pressure. Four pumps are used to exhaust the neutral particles generated at the device wall through the recombination process. The two buffle plates protect the back-flow of the neutral particles from end wall to plasma bulk region, and are located at z=720 and 3240 mm. Background vacuum pressure measured with two ionization gauges is a few times of 10^{-4}Pa with the effective exhaust velocity of 1000 l/s. During discharge, neutral pressure is measured with two manometers located at z=0.5, 2.14m.

2.5 Numerical Linear Device

Three-dimensional numerical simulation code of the resistive drift wave turbulence in a linear device, called Numerical Linear Device (NLD) has been developed [3]. We review it for illastrating the plasma turbulence of concern. The three-field (density, potential, and parallel velocity of electrons) reduced fluid model is adopted. The plasma has a simple cylindrical shape, and the magnetic field has only the component in the axial direction

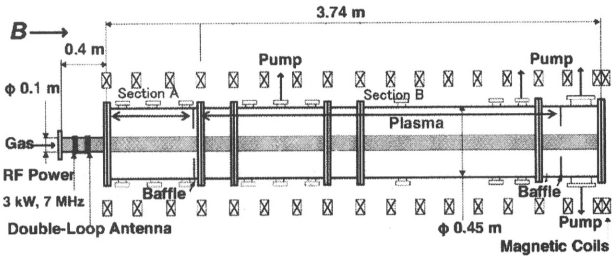

Fig. 3 Equatorial mid-plane of LMD-U

Parameters	Typical Value	Range
Base Pressure (Source)	$4.5\cdot10^{-3}$ Pa	$7.0\cdot10^{-4}$-$3.0\cdot10^{-3}$ Pa
Neutral Gas Pressure (Argon)	2 mTorr	1.5-6 mTorr
	0.35 Pa	0.26-1.07 Pa
Magnetic Field	900 G	100-1500 G
RF Power	3 kW	0.5-5 kW
Peak Electron Density	$6\cdot10^{18}$ m^{-3}	10^{18}-10^{19} m^{-3}
Electron Temperature	3 eV	2-4 eV

Fig. 4 Typical operational condition and plasma parameters for the LMD-U

with the uniform intensity. According to experiments, high density ($n_e \geq 1 \times 10^{19}\mathrm{m}^{-3}$) and low temperature ($T_e < 5\mathrm{eV}$) plasmas in an argon discharge are analyzed. The density of neutral particles is high even in the plasma core region, so the effect of neutral particles is taken into consideration. The continuity equation, the vorticity equation, and Ohm's law can be used to obtain the fluctuating density, potential, and parallel velocity of electrons[20],

$$\frac{dN}{dt} = -\nabla_{\parallel} V - V\nabla_{\parallel} N + \mu_N \nabla_{\perp}^2 N + S_N \qquad (2.15)$$

$$\frac{d\nabla_{\perp}^2 \phi}{dt} = \nabla N \cdot (-\nu_{in}\nabla_{\perp}\phi - \frac{d\nabla\phi}{dt})$$

$$-\nu_{in}\nabla_{\perp}^2\phi - \nabla_{\parallel} V - V\nabla_{\parallel} N + \mu_W \nabla_{\perp}^4 \phi \qquad (2.16)$$

$$\frac{dV}{dt} = \frac{M}{m_e}(\nabla_{\parallel}\phi - \nabla_{\parallel} N) - \nu_e V + \mu_V \nabla_{\perp}^2 V \qquad (2.17)$$

where $N = ln(n/n_0)$, $V = v_{\perp}/c_S$, $\phi = e\varphi/T_e$, n is the density, n_0 is the density at r=0, $v_{\parallel}$ is the electron velocity parallel to magnetic field, c_S is the ion sound velocity, φ is the electrostatic potential, T_e is the electron temperature, $d/dt = \partial/\partial t + [\phi]$ is the convective derivative, S_N is a particle source term, M/m_e is mass ratio of the ion and electron, ν_{in} is the ion-neutral collision frequency, $\nu_e = \nu_{ei} + \nu_{en}$ is the sum of the ion-electron and electron-neutral collision frequency, and μ_N, μ_V and μ_W are artificial viscosities. The ion cyclotron frequency Ω_{ci} and Larmor radius measured by the electron temperature ρ_S are used for the normalizations. The equations are solved in the cylindrical coordinate with spectral expansion in the azimuthal and axial directions assuming periodic boundary condition, where m and n are the azimuthal and axial mode number, respectively. The boundary condition in the radial direction are set to f=0 at r=0, a when $m \neq 0$, and $\partial f/\partial r$=0 at r=0, f=0 at $r = a$ when m=0, where f implies $\{N, \phi, V\}$, and $r = a$ gives an outer boundary of the plasma column. Fig. 5-7 show time evolution of fluctuating potential(5), density(6), and parallel velocity(7) on a azimuthal cross-section of LMD-U plasma.

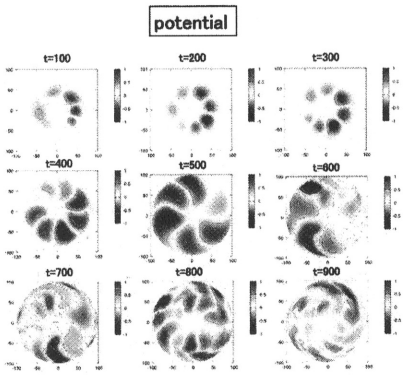

Fig. 5 Time evolution of electrical potential fluctuation. Here t is normalized by ion cyclotron frequency.

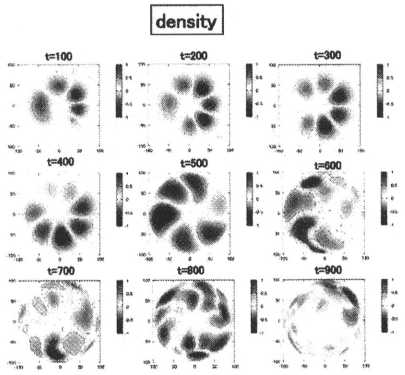

Fig. 6 Time evolution of density fluctuation. Here t is normalized by ion cyclotron frequency.

3. Simulation

3.1 Model Equations

Nonlinear two-dimensional code calculating steady state neutral density in a linear device was developed.

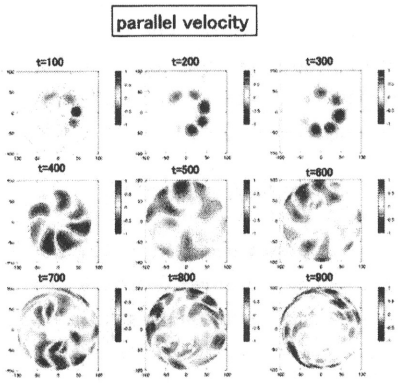

Fig. 7 Time evolution of parallel velocity fluctuation. Here t is normalized by ion cyclotron frequency.

The code uses Monte Carlo algorithm and takes experimental data in LMD-U as input parameters. Schematic view of the LMD-U are shown in Fig.3. Possible methods of controlling the number of neutrals in a LMD are investigated by numerical evaluation of the Boltzmann equation for various atomic processes. In the simulation, the system is considered to be two-dimensional, since a LMD consists of a plasma productiontube and a cylindrical main chamber connected in series. Although some equipments like vacuum pumps break the axisymmetry, their ports are small and the profile in the axial direction is of primary importance in studying neutral transport. In addition, the plasma is assumed to be uniform in the axial direction. In future, the simulation model will be upgraded to include the two- or three-dimensional plasma profiles.

3.1.1 Governing Equations

In a steady state, a statistical distribution of neutral particles $f_n(\mathbf{r}, \mathbf{v})$ is described by the Boltzmann equasion:

$$\mathbf{v}\frac{\partial f_n}{\partial \mathbf{r}} = C(f_n) + S \ , \tag{3.1}$$

where $\mathbf{v}$ is the particle velocity, $C(f_n)$ is the collision term and S is the source term. For the present calculation, balance between the distributions of incident $f_{n,inc}$ and reflected $f_{n,rfl}$ particles is fulfilled at the boundary[12]:

$$f_{n,rfl}\,|_{\mathbf{r}=\mathbf{r}_{bnd}} = [\boldsymbol{R}_s f_n(v_\perp \rightarrow -v_\perp) + \boldsymbol{R}_d \boldsymbol{\Gamma}_{inc} \boldsymbol{F}_d]|_{\mathbf{r}=\mathbf{r}_{bnd}} \ . \tag{3.2}$$

Here, the vector $\boldsymbol{r}_{bnd}$ points to the boundary (chamber walls, baffle plate, end plate, source positions, or pump ducts), $v_\perp$ is the component of the incident particle velocity toward the boundary, $\boldsymbol{R}_s$ and $\boldsymbol{R}_d$ are the coefficients of specular and diffusive reflection, respectively, $\boldsymbol{\Gamma}_{inc} = \int \mathbf{v}_\perp f_n(v_\perp > 0) d\mathbf{v}$ is the flux of the neutrals towards the wall and the distribution of the diffusively emitted particles $\boldsymbol{F}_d$ is normalized by $\int_0^\infty v_\perp \boldsymbol{F}_d d\mathbf{v} = 1$. At the pump duct position, the specular reflection coefficient $\boldsymbol{R}_s$ is replaced by $1 - \gamma$ where γ is the pump efficiency. In general, all parameters on the right-hand side are functions of the particle velocities and positions. In contrast to the conventional calculations of fusion plasmas, in the case of the simulated linear device, the neutral self-collisions $C_n(f_n, f_n)$ are expected to play an important role due to the high neutral density, making the Boltzmann equation nonlinear. As well as the self-collisions, electron impact ionization $C_e(f_n, f_e)$ significantly affects the neutral profiles. To take into account the energy transport from ions to neutral particles, the elastic ion-neutral collisions $C_i(f_n, f_i)$ are also considered:

$$C(f_n) = C_n(f_n, f_n) + C_e(f_n, f_e) + C_i(f_n, f_i) \ , \tag{3.3}$$

with

$$C_n(f_n, f_n) = \iint \boldsymbol{I}_{els}(u, \Omega) u (f_n' f_n' - f_n f_n) d^3 v_2 d\Omega \ , \tag{3.4}$$

$$C_e(f_n, f_e) = \iint \boldsymbol{I}_{mom}(u, \Omega) u (f_n' f_i' - f_n f_i) d^3 v_2 d\Omega + \iint \boldsymbol{I}_{cxr}(u, \Omega) u (f_n' f_i' - f_n f_i) d^3 v_2 d\Omega \ , \tag{3.5}$$

$$C_i(f_n, f_i) = -\iint \boldsymbol{I}_{ion}(u, \Omega) u f_n f_e d^3 v_2 d\Omega \ , \tag{3.6}$$

where $\boldsymbol{I}_{els}$, $\boldsymbol{I}_{mom}$, $\boldsymbol{I}_{cxr}$ and $\boldsymbol{I}_{ion}$ are the self-elastic, ion momentum transfer, resonance charge exchange and electron impact ionization differential cross sections, respectively, f_e and f_i are the electron and ion distribution functions, respectively, $u = |\mathbf{v}_1 - \mathbf{v}_2|$, $\mathbf{v}_1$ and $\mathbf{v}_2$ are the incident and the target particle velocities, respectively, and Ω is the scattering solid angle. The distribution functions of the scattered particles are marked by primes[13].

The linear collision term C_i and C_e can be reduced to simplified forms by assuming isotropic scattering: $\boldsymbol{I}(u, \Omega) = \boldsymbol{I}(u)$. In this case, integration over the solid angle is performed explicitly, and the differential cross sections $\boldsymbol{I}(u)$ are replaced by the corresponding total cross sections $\sigma(u) = \int \boldsymbol{I}(u) d\Omega = 4\pi \boldsymbol{I}(u)$. Next, note that the electron speed $|\mathbf{v}_e|$ is clearly much larger than that of neutrals $|\mathbf{v}_n|$. Therefore, in the case of impact ionization, the relative speed is given by $u = |\mathbf{v}_e|$ and ionization collision term reduces to

$$C_n(f_n, f_e) = -n < \sigma_{ion} u > f_n \ , \tag{3.7}$$

where $< \sigma_{ion} u >= \int |\mathbf{v}_e| \sigma_{ion}(|\mathbf{v}_e|) F_e(\mathbf{v}_e) d^3 v_e$ is the ionization rate coefficient, and the distribution function f_e is assumed to be the product of the electron density n_e and the electron velocity distribution F_e.

In the case of the ion collision term, the products $\sigma_{mom}(u)u$ and $\sigma_{cxr}(u)u$ are slowly varying functions of the relative velocity in the region of interest, and thus they can be placed outside the integrands[12][14]:

$$C_i(f_n, f_i) = n_i(< \sigma_{mom}(u)u > + < \sigma_{cxr}(u)u >) \times [F_i(\mathbf{v}\mathbf{V}_i) \int f_n(\mathbf{v}') d^3 v' - f_n(\mathbf{v})] \ , \quad (3.8)$$

where $f_i = n_i F_i$ with n_i being the ion density and F_i being the ion velocity distribution; the mean ion velocity $\mathbf{V}_i$ is shown explicitly.

In contrast to the linear collision integrals, eq.(3.5) and (3.6), the neutral self-collision term cannot be easily simplified because of its nonlinear nature. In this article, a stationary state is searched for, and the nonlinear operator $C_n(f_n, f_n)$ is treated by interations:

$$\mathbf{v} \frac{\partial f_{n,k+1}}{\partial \mathbf{r}} = C_n(f_{n,k+1}, f_{n,k}) + C_i(f_{n,k+1}, f_i) + C_e(f_{n,k+1}, f_n) + S_{k+1} \ , \quad (3.9)$$

where k is the iteration number. In this case, the C_n term 繰 in each iteration step is calculated using the distribution of the previous step distribution and thus it becomes linear. Therefore, within each iteration step it can be written in a similar form to eq.(3.8)

$$C_n(f_{n,k+1}, f_{n,k}) = n_{n,k} < \sigma_{els}(u)u > \times [F_{n,k}(\mathbf{v}\mathbf{V}_n) \int f_{n,k+1}(\mathbf{v}') d^3 v' - f_{n,k+1}(\mathbf{v})] \ , \quad (3.10)$$

where $f_{n,k} = n_{n,k} F_{n,k}$ and $N_{n,k}$ and $F_{n,k}$ are the neutral density and velocity distribution obtained from the previous iteration step respectively, and V_n is the neutral mean velocity.

In the iteration scheme, the zeroth order test function $f_{n,0} = n_{n,0} F_{n,0}$ can be chosen arbitrarily. In the present simulation, the zeroth-order neutral profile $n_{n,0}$ is taken to be uniform, $n_{n,0} = \int_{inj} \Gamma_{inj} d^2 r / P$ and the velocity distribution is $F_{n,0} = \delta(v - v_{th})$, where Γ_{inj} is the injected particle flux, P is the pumping speed, $v_{th} = \sqrt{2 k_B T_n / M_n}$ is the most probable speed of neutrals, k_B is Boltzmann's constant, T_n is the nertral temperature and M_n is the mass of a nertral particle. Here, the zeroth-order mean velocity is assumed to be zero. Rigorously speaking, the final converged solution ($k \to \infty$) may depend on the choice of the initial conditions at k=0. Such critical dependence on the initial conditions was not found.

To complete the definition of the problem, the source term S has to be explained. The neutral particles are assumed to be originated from gas injection S_{inj}, from the recombination of ions at the end plate, S_{ep}, and from the plasma itself, S_{pl}:

$$S = S_{inj} + S_{ep} + S_{pl} \ , \quad (3.11)$$

where S_{inj} is the prescribed term of the injected particles, and S_{ep} can be obtained from the distribution of charged particles and the properties of the end plate. To determine S_{pl}, a steady-state condition is used. Namely, the ionization rate is equal to the recombination rate:

$$\iint C_e d^3 v d^3 r = \iint S_{ep} d^3 v d^3 r + \iint S_{pl} d^3 v d^3 r \ , \quad (3.12)$$

where the integrals are calculated over the plasma volume. The first term on the right-hand side of eq. (3.12) is the number of neutral particles originating on the end plate per second due to the recombination of ions:

$$J_{ep} = \int_{ep} n_i V_{i\perp} d^2 r \ , \quad (3.13)$$

where $n_i V_{i\perp} = \Gamma_{i,ep}$ is the ion particle flux at the end plate and the plasma flow is assumed to be made by only the ion drift. The integral is evaluated over the end plate surface. All ions at the end plate are assumed to be neutralized i.e., $\iint S_{ep} d^3 v d^3 r \equiv \Gamma_{n,ep} = \Gamma_{i,ep}$.

Finally, from eq.(3.12) and (3.13) the number of particles being originated in the plasma is due to recombination J_{pl}

$$J_{pl} = \iint C_e d^3 v d^3 r - \int_{ep} n_i V_{i\perp} d^2 r \ . \quad (3.14)$$

The latter expression does not provide information regarding the position of the originated particles. In the present analysis, for the sake of simplicity, recombination inside the plasma is replaced by that at the radial plasma boundary, and the particles are distributed uniformly in the axial and azimuthal directions. The direction and speed of the new particles can be chosen on the basis of physical reasons or assumptions. In the present version of the code, all source particles have a speed of v_{th} and are directed randomly.

3.1.2 Monte Carlo Method

To obtain the neutral gas density distribution in the linear device, the Boltzmann equation [eq. (3.1)] is numerically evaluated by the Monte Carlo method. A general discussion of the method and the applocation of the algorithm to the neutral profile calculations can be found elsewhere. Here, only a brief outline of the method is presented[14-18].

During the simulation, N_{src} test flights with an initial dimensionless weight of $\omega = 1$ are generated for each

source. Here, the subscript "src" is given to terms regarding the injected neutrals ("inj") and particles recombining on the endplate ("ep") or in the plasma ("pl "). If the source produces $J_{src}\mathrm{s}^{-1}$, then each flight is represented by $J_{src}/N_{src}\mathrm{s}^{-1}$ at its start.

For the present calculation, the number of injected particles J_{inj} is a prescribed value, chosen from the conditions of the experiment. The number of particles originating at the endplate, J_{ep}, is given by eq. (3.13) and that of particles originating at the plasma surface, J_{pl}, is defined by eq. (3.14), which is transformed into

$$J_{pl} = \frac{\kappa_{inj,ion} J_{inj} - (1 - \kappa_{ep,ion}) J_{ep}}{1 - \kappa_{pl,ion}} , \qquad (3.15)$$

where $\kappa_{src,ion} = \Sigma_j \omega_{(src,ion),j}/N_{src}$ is the fraction of ionized particles for each source type, $\omega_{(src,ion),j}$ is the weight of the ionized particle and a summation is taken over all ionized particles. The sign of J_{pl} can be used as a test parameter; a negative J_{pl} indicates that the input parameters are incorrect.

Each flight follows its trajectory with a prescribed short step dl. At each step, collision events are tested one after another.

(1) First, the elastic self-collision event is checked: if $rnd_1 < dl/\lambda_{els}$ holds, then the event has occurred and a new direction of propagation is randomly chosen. Here, rnd_1 is uniformly distributed random number(URN), $\lambda_{els} = 1/(\sqrt{2} n_n \sigma_{els})$ is the self-collision mean free path(MFP), $\sqrt{2}$ takes the relative motion of the neutrals into accout.

(2) Next, if $rnd_2 < dl/\lambda_{mom}$ holds, where rnd_2 is URN and $\lambda_{mom} = v_n/[\bar{u_i} n_i(\sigma_{mom} + \sigma_{chr})]$ is the ion-neutral collision MFP (v_n is the speed of the test particle and $\bar{u_i}$ is the average ion speed), then an ion elastic collision has occurred. In this case, the speed of the flight becomes equal to $V_{i,drift}$ and a new direction is randomly chosen.

(3) Finally, if $rnd_3 < dl/\lambda_{ion}$ where rnd_3 is a URN and $\lambda_{ion} = v_n/(n_e \langle \sigma_{ion} u \rangle)$ is the ionization MFP, then a ionization event has occurred and $\omega = 0$.

(4) If there is no collision, then the flight makes the next step in the previous direction. All events are put in order of importance. The self-elastic collision changes the direction of the flight but does not change the particle energy and weight, and it is tested first. The ion-elastic collision ffects the particle speed but does not change the particle weight. The ionization can significantly affect the neutral profile, and therefore it is checked last. The proposed scheme allows us to accurately examine the ionization rate, even if the neutral density is high and the step dl is comparable to the total MFP.

The exhaust by the vacuum pump is simulated by reducing the weight of the test flight that hits the pump duct area:

$$\omega_{rft} = \begin{bmatrix} \omega_{inc}(1 - P/(S_{pmp} v_\perp)) & P/(S_{pmp} V_\perp < 1 \\ 0 & P/(S_{pmp} v_\perp) < 1 \end{bmatrix} , \qquad (3.16)$$

where ω_{rfl} and ω_{inc} are the weights of the flight after and before hitting the pump, P is the pumping speed, S_{pmp} is the pump duct area and $v_\perp$ is the component of the flight velocity normal to the pumping duct surface.

The flight is traced until its weight becomes smaller than a prescribed threshold. The calculation domain is divided into cells, and at each flight step various data are accumulated at the corresponding cell. At the end of each iteration, the accumulated data are transformed into physical quantities. For example, the average neutral density can be obtained as

$$\bar{n}_n(l) = \frac{dl}{V(l)} \sum_{src} \frac{J_{src}}{N_{src}} \sum_{fligths} \frac{\omega(l)}{|\mathbf{v}_n(l)|} , \qquad (3.17)$$

where l is the number of the cell, $\mathbf{v}_n(l)$ is the velocity of the test flight at the cell location, V is the volume of the cell, and summation is taken over all flights passing through the cell. Similarly, the average component or absolute value of the neutral velocity is

$$\bar{v}_{n,j}(l) = \frac{dl}{\bar{n_n}(l) V(l)} \sum_{src} \frac{J_{src}}{N_{src}} \sum_{fligths} \frac{\omega(l) v_{n,j}(l)}{|\mathbf{v}_n(l)|} , \qquad (3.18)$$

Here, $v_{n,j}$ is the component or absolute value of the test flight velocity at the cell location.

3.1.3 Validation of the Model

First, the iteration algorithm is validated. For this, the diffusion of neutral gas in a cylindrical tube without plasma is considered. The length of the tube is L and the radius is r_{tube} . At the rear side of the tube, a semipermeable membrane with reflection coefficient R is located. Every second, particles are injected into the tube uniformly. The front and radial walls are assumed to be perfect reflectors; hence, the particles can only leave the tube through the membrane. An analytical expression for the neutral density can be obtained from steady-state one-dimensional continuity equation:

$$\frac{d\Gamma}{dz} , \qquad (3.19)$$

where Γ is the constant stream flux, A neutral gas with a high density is considered, such that the MFP is much shorter than a characteristic system size. The semipermeable membrane is assumed to introduce a constant gas stream Γ_0. In this case, the flux is given by the diffusion and streaming terms:

$$\Gamma = \Gamma_0 + D \frac{dn_n}{dz} . \qquad (3.20)$$

where $D = \bar{v_n}/(3\sqrt{2}n_n\sigma_{els})$ is the diffusion coefficient, and $\bar{v_n} = \sqrt{8k_bT_n/(\pi M_n)}$ is the average speed of propagation of the neutrals. Therefore, from eqs. (3.19) and (3.20), profile is determined as

$$n_n(z) = n_n(0)e^{-z/\lambda_{eff}} , \qquad (3.21)$$

where λ_{eff} is the effective MFP, which is determined from boundary conditions, together with $n_n(0)$

Indeed, at the boundary, the particle fluxes are prescribed. From the steady-state condition, the total flux through any tube section is constant and is equal to the influx. Therefore,

$$\Gamma|_{z=0} = \Gamma_{inj} , \qquad (3.22)$$

where $\Gamma_{inj} = J_{inj}/(\pi r_{tube}^2)$.

At the membrane position, the fluxes of the reflected and the incident particles how the relation to each other through the reflection coefficient, giving a total flux of[19]

$$\Gamma|_{z=L} = \frac{n_n\bar{v}_n}{2}\frac{1-R}{1+R} . \qquad (3.23)$$

Equations (3.20)-(3.23) allow us to obtain the neutral density for given Γ_0. For the sake of the model validation, the definition of the particle flux through the mean flow speed of particles is more conveniently given as

$$\Gamma = n_nV_d . \qquad (3.24)$$

In this case, at the boundaries:

$$n_nV_d|_{z=0} = \Gamma_{inj} , \qquad (3.25)$$

$$V_d|_{z=L} = \frac{\bar{v}_n}{2}\frac{1-R}{1+R} , \qquad (3.26)$$

$$n_n|_{z=L} = \frac{2\Gamma_{inj}}{\bar{v}_n}\frac{1+R}{1-R} , \qquad (3.27)$$

Equations (3.21), and (3.25)-(3.27) form the analytical statement of the problem and can be solved. The set is not a closed one, since the boundary conditions depend on the flow speed V_d, which is not determined. Therefore, the solution has a unknown parameter,

$$n_n = \frac{\Gamma_{inj}}{V_d|_{z=0}}\left(\frac{V_d|_{z=0}}{V_d|_{z=L}}\right)^{z/L} , \qquad (3.28)$$

here, $V_d|_{z=L}$ is determined by eq. (3.26) and $V_d|_{z=0}$ is the parameter. Nevertheless, the analytically obtained solution can be compared with the numerical one. First of all, at the exhaust port, the flow speed and neutral density depend on the input parameters only, and thus they can be directly compared with the results of simulation. Then, from the numerical calculations, it is possible to determine the parameter $V_d|_{z=0}$ and therefore the shapes of the analytical and numerical solutions can be also compared, as shown in Fig.8. Here, arrows indicate the neutral density obtained using eq. (3.27). Symbols show the radially averaged numerical neutral profiles, and lines show the analytical solutions obtained from the mean speed of the particles in the simulation.

During the simulation, to ensure that λ_{els} is much smaller than the dimensions of the tube, the number of injected particles is chosen to be $J_{inj} = 2.0 \times 10^{21}\mathrm{s}^{-1}$, with tube length L=2m and radius r_{tube}=0.5m. The relative error between the analytical and numerical solutions in the main region is within 5%. Only close to the boundaries the error is large, since the solution [eq. (3.28)] is not valid here due to the lack of interparticle collisions. The results demonstrate that the numerical algorithm is able to accurately calculate the shape and value of the profile for a wide range of reflection coefficients.

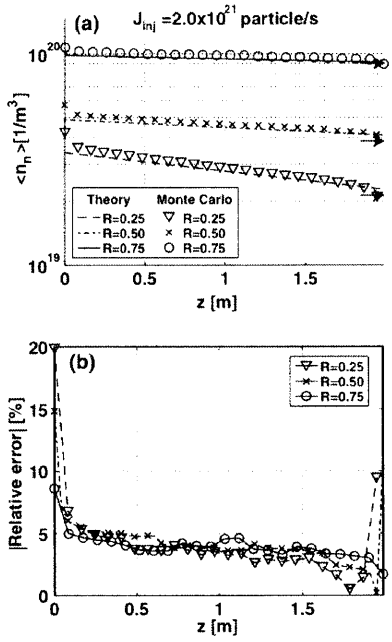

Fig. 8 (a) Racially averaged numerical (symbols) and analytical neutral profiles (lines) $\langle n_n \rangle$ and (b) relative error of calculation. The number of the injected particles is $J_{inj} = 2.0 \times 10^{21}\mathrm{s}^{-1}$, L = 2m, and r_{tube}=0.5m. Arrows indicate values obtained using eq.(3.27)

3.2 Simulation Results

It is reported that neutral pressure profile is very sensitive to the electron density and the temperature

profile. The n_e and T_e, which are taken into account in the simulations, can be measured experimentally. Typical electron temperature and density of LMD-U plasmas are $3-5$ eV and $0.5-1.0\times10^{19}\mathrm{m}^{-3}$, respectively. Other parameters such as ion temperature and speed of plasma flow are difficult to be measured, thus, typical values of ion temperature $T_i = 0.2 - 1.0$ eV and plasma Mach number $M_n = 0.01 - 0.3$ are used.

Figure 9 shows radially averaged neutral pressure for injected argon flux of Γ_n=$6.4\times10^{19}\mathrm{s}^{-1}$, $9.7\times10^{19}\mathrm{s}^{-1}$ and $12.9\times10^{19}\mathrm{s}^{-1}$. Two baffle plates are installed in the LMD-U to control the neutral pressure. The simulation results show sharp changes of the neutral pressure at the baffle positions. The increase in the neutral pressure near the end plate (z=3.74m) is resulted from a neutral particle source due to the recombination of plasma. In the central region (Section B), the neutral pressure decreases with the increase of the Mach number. Thus the Mach number is known to be an important parameter to determine the P_n profile. The information about plasma flow is hardly obtained in LMD-U experiments, thus the dependence of neutral pressure on Mach number in the simulation is necessary and is investigated. To compare the simulation results with experimental observations, neutral pressures at z=0.5m and z=2.14m, where manometers are installed, are calculated. The neutral pressures at above positions represent one in the sections A and B of LMD-U (see Fig.3), respectively. Figure 10 shows Mach number dependence of neutral pressure for three different T_e conditions. The T_e and M_n dependences of P_n are different at the section A and B. This fact suggests that if P_n in the sections A and B are measured, T_e and M_n should be chosen to explain the P_n in both sections, simultaneously. The observed P_n level is shown in Figure 10 by the dashed horizontal lines, for an exmple. A condition with T_e=$3-5$eV, Mach number M_n ~$0.2-0.3$ and injected neutral flux Γ_n=$6.4\times10^{19}\mathrm{s}^{-1}$ can be consistent with the experimental results in both sections. In the Mach number region of $0.1\leq M_n\leq0.3$, the T_e dependence of P_n is very weak in both sections. The choice of T_e and M_n from simulations have large ambiguity and is impossible in reality. When the experimental observation of T_e ~3eV is employed, M_n can be obtained more precisely. For the case of Γ_n=$9.7\times10^{19}\mathrm{s}^{-1}$ case, the T_e dependence of P_n is stronger than that for Γ_n=$6.4\times10^{19}\mathrm{s}^{-1}$ case. Thus, T_e and M_n can be obtained more precisely from simulation results in this case. The simulation results are insensitive to the density n_e as shown in Figure 11 and 12. The M_n dependense of P_n is also affected by T_i. Figure 13 shows that the increase in the T_i increases P_n, and this T_i dependence of P_n is affected by T_e quantitatively. The density dose not affect this T_i dependence,

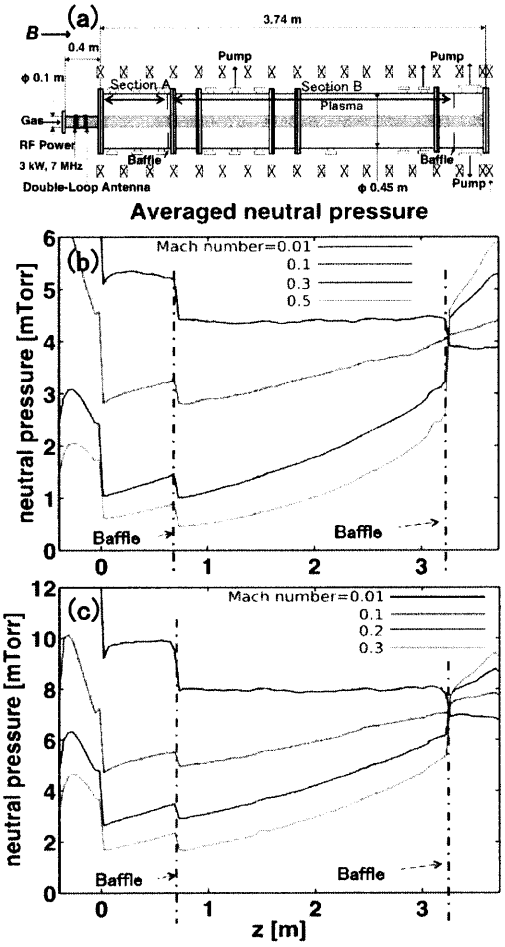

Fig. 9 (a) The schematic view of LMD-U and typical simulated neutral pressure profile for (b) Γ_n = 6.4 $\times10^{19}\mathrm{s}^{-1}$ and (c) Γ_n = 9.7 $\times10^{19}\mathrm{s}^{-1}$. Here T_e=3eV, n_e=0.5 $\times10^{19}\mathrm{s}^{-1}$, T_i=0.5eV

as shown in Fig. 14. The T_i dependence of P_n is strong in the typical range of T_i ($0.2\leq T_i\leq1$eV). Thus, there is a possibility to obtain T_i from Mach number, injected neutral flux and T_e. A condition of Mach number M_n=0.2, T_e=3eV, injected neutral flux Γ_n=$6.4\times10^{19}\mathrm{s}^{-1}$ yields T_i=0.5eV in the section A. This T_i value is considered to be reasonable compared to the value obtained from spectroscopy in similar linear plasmas.

4. Comparison with Experimental Results

In this chapter, simulation results are compared with experiments. There are two experimental knobs to control the neutral pressure namely the injected neutral flux and pumping speed in LMD-U. To validate the simulation model, the qualitative comparison in the wide range of experimental condition is necessary. Thus ex-

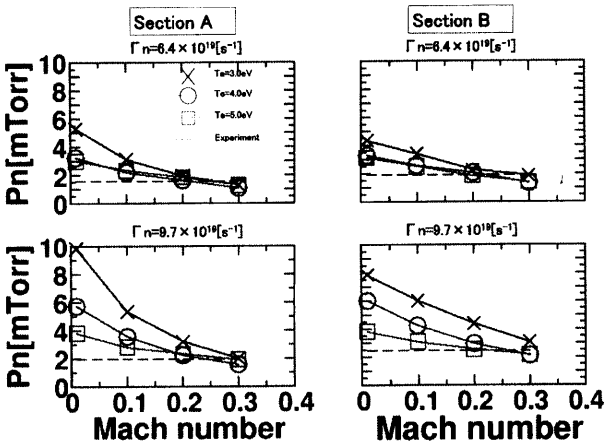

Fig. 10 Mach number dependence of simulated neutral pressure for three different T_e conditions.(T_e=3eV, 4eV, 5eV) at different values of Γ_n=6.4×10^{19}s^{-1} and Γ_n=9.7×10^{19}s^{-1}, here T_i=0.5eV.

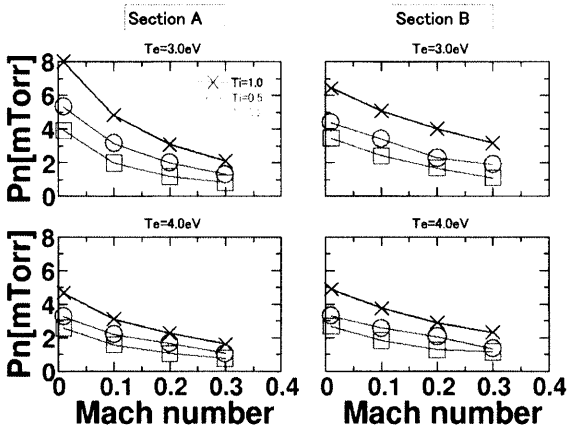

Fig. 12 Dependence of neutral pressure at z=0.5m and 2.14m on Mach number for three different T_i conditions T_i=1.0eV, 0.5eV and 0.2eV, where Γ_n = 6.4 ×10^{19}s^{-1}, T_e=3eV and 4eV, n_e=0.5×10^{19}m^{-3}.

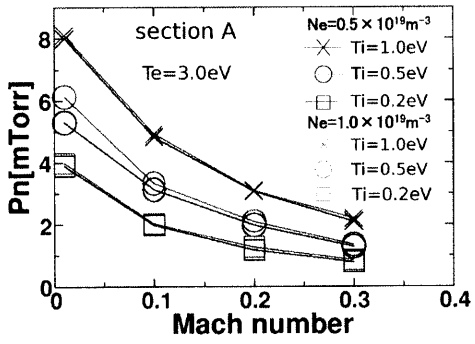

Fig. 13 Dependence of neutral pressure at z=0.5m on Mach number for three different T_i conditions T_i=1.0eV, 0.5eV and 0.2eV and for two different n_e conditions n_e=0.5×10^{19}m^{-3} and n_e=1.0×10^{19}m^{-3}, where Γ_n = 6.4 ×10^{19}s^{-1}, T_e=3eV.

Fig. 11 Dependence of neutral pressure at z=0.5m on Mach number for two different n_e conditions n_e=0.5×10^{19}m^{-3} and n_e=1.0×10^{19}m^{-3} for T_e=3eV and 4eV, where Γ_n = 6.4 ×10^{19}s^{-1}.

periments changing the injected neutral flux and the pumping speed are performed.

4.1 Experimental Setup

In this study, the two manometers are installed to measure the neutral pressures in the different sections (section A and B) of vacuum chamber, as shown in Figure 3. Section A and section B are separated by a baffle plate, and thus a comparison between two manometer signal is also useful to check the function of the baffle plate. Figure 14 shows a typical time evolution of neutral pressures measured by manometers. The ion saturation current is also indicated as an index of the time evolution of plasma density. Manometer installed in the section A indicates that the neutral pressure tends to decreases in the latter period of discharge and then saturated. On the other hand, one in the section B tends to increase during the discharge. In this study, we use the value of P_n at t=500ms to discuss the saturation level of the neutral pressure. The dynamics of neutral pressure is one of the most important subjects of future works.

4.2 Pumping Speed Dependense

Pumping speed of LMD-U was also changed. In this experiment, injected neutral flux, heating power and magnetic field are kept constant. Comparisons between

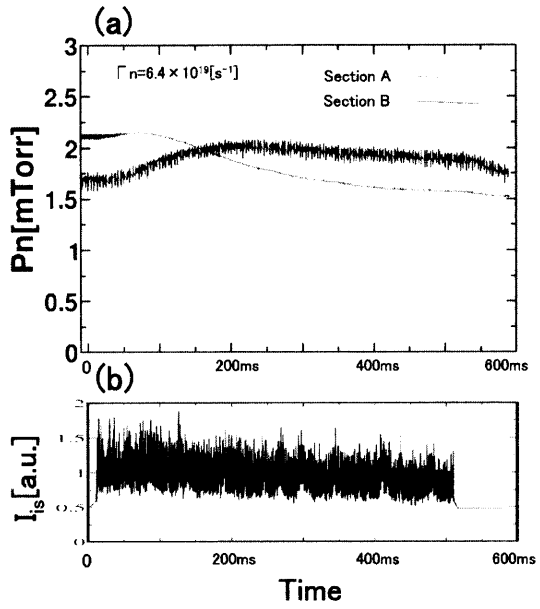

Fig. 14 (a) Typical time evolution of neutral pressure and (b) ion saturation current.

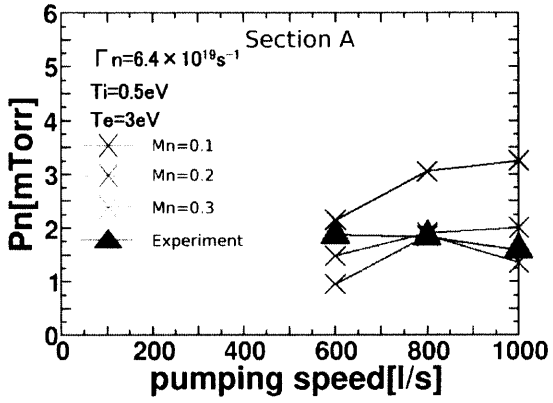

Fig. 15 Neutral pressure as a function of pumping speed in experiment is plotted by filled triangles and the simulational values are plotted by crosses.(at Section A)

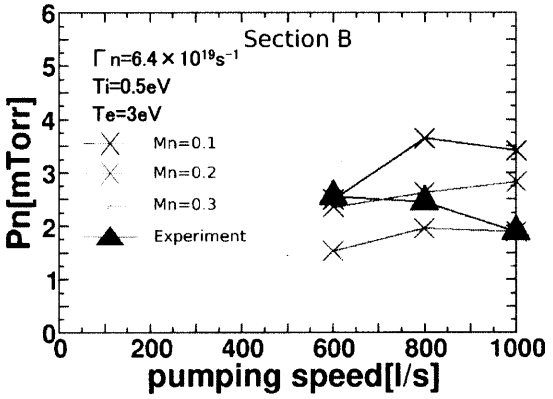

Fig. 16 Neutral pressure as a function of pumping speed in experiment is plotted by filled triangles and the simulational values are plotted by crosses.(at Section B)

simulation and experimental results are shown in Figure 15 and 16. The observed neutral pressure decreases monotonically with increase in the pumping speed v_{pmp}. The qualitative features obtained from simulation and experiment are slightly different. Experimental results can be consistent with simulation results quantitatively under the assumption of T_e=3eV and $M_n = 0.1 - 0.3$. This assumption is also consistent with neutral pressure behavior not only in the section A but also in the section B. The simultaneous two-point measurement of neutral pressure may not deny a validity of this assumption. The simulation of M_n=0.3 can fit the experimental result in the pumping speed v_{pmp}=1000 l/s case. And simulation of M_n=0.1 can fit the experimental result in the v_{pmp}=600 l/s case. This result suggests that an increase in the pumping speed can increase the Mach number. For more precise comparison between simulation and experiment, the direct measurement of M_n is neccesary.

4.3 Injected Neutral Flux Dependense

Next, the injected neural gas flux is changed, here the pumping speed is kept to 1000 l/s. Figures 17 and 18 show the value of neutral pressure P_n, as a function of the injected neutral flux Γ_n. In the large neutral flux case (Γ_n >14×10^{19}s^{-1}), the convergence of numerical calculation is not sufficient thus they are not shown. In the smaller neutral flux cases, the simulational results are consistent with experimental ones not only qualitatively but also quantitatively except for Γ_n=9.7×10^{19}[s^{-1}]. The tuning of T_e, T_i, M_n may be required for more precise comparison between simulational calculations and experimental observations.

The simulational results show that the neutral pressure is inhomogeneous along z-axis. The neutrals contribute to plasma density and thus the plasma may become inhomogeneous along the magnetic field. In simulation model, such an inhomogeneity of plasma is not taken into account. Simulation model is still useful to obtain approximate values of M_n and T_i. The neutral pressure profile obtained from this simulation, therefore, can be applied as input and/or boundary conditions to another simulation codes e.g. NLD.

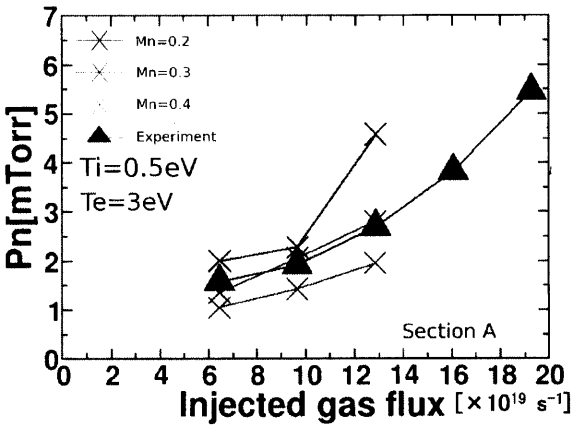

Fig. 17 The value of neutral pressure P_n is plotted against the injected particles Γ_n in experimental value is shown by blue and simulational values are shown by black and red for three different of M_n=0.2, 0.3, and 0.4, T_e=3eV. (at Section A)

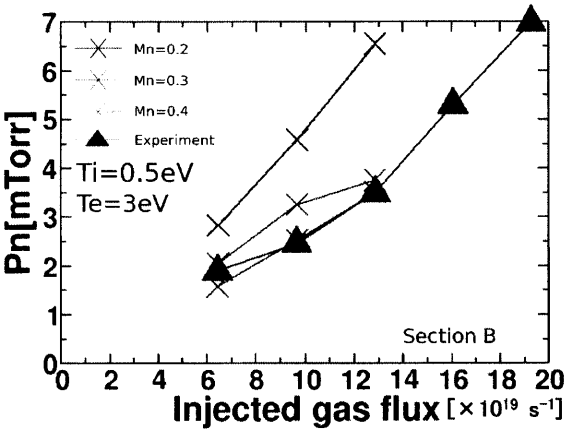

Fig. 18 The value of neutral pressure P_n is plotted against the injected particles Γ_n in experimental value is shown by blue and simulational values are shown by black and red for three different of M_n=0.2, 0.3, and 0.4, T_e=3eV.(at Section B)

5. Summary

Behavior of neutral pressure in LMD-U is investigated by numerical simulation and experiment. In the simulation code, the Boltzmann equation is solved by Monte Carlo method and Mach number dependence of neutral pressure is obtained. The simulated results of neutral pressure for the different sections of vacuum chamber of LMD-U are compared to the experimental observations.

Obtained results in this study are summarized as follows:

1) In the simulational study, we observe that the neutral pressure decreases monotonically with the increase of the Mach number, M_n.

2) The Mach number M_n dependence of neutral pressure P_n is not apparently affected by the electron density n_e.

3) Increases in both the electron temperature T_e and decreases in the ion temperature T_i decrease the Mach number M_n. The T_i dependence of P_n is found strong in the region of $0.2 \leq T_i \leq 1.0$ eV.

4) The two-point simultaneous observation of P_n is performed in LMD-U.

5) The two-point observation of P_n can be fitted to the simulation results under appropriate assumptions of M_n, T_e and T_i.

6) The simulation with appropriate assumptions of M_n, T_e, T_i values can be consistent with the experimental results ((a)injected neutral flux dependence and (b)pumping speed dependence).

Turbulence structure observed in LMD-U strongly depends on the neutral pressure. For quantitative understanding of turbulence structure formation mechanism, precise values of many parameters are required. Establishment of a dependable simulation code is necessary and useful to determine parameter values which are difficult to be observed directly. This study partially demonstrates a validity of our neutral transport code by the comparison study with experiments.

Acknowledgements

We thank Dr. M. Azumi, Dr. N. Kasuya and Dr. M. Ignatenko for useful comments on this paper. This work is partly supported by the Grant-in-Aid for Specially-promoted Research (16002005), by the Grant-in-Aid for Scientific Research B (16360459) and by the collaboration programs of NIFS and of the Research Institute for Applied Mechanics of Kyushu University.

References

1) M. Ignatenko, M. Azumi, M. Yagi, S. Shinohara, S. -I. Itoh, and K. Itoh, Jpn. J. Appl. Phys., Part 1 **46**, 1680 (2007).
2) M.Ignatenko, M.Azumi, M.Yagi, S.Shinohara, S.-I.Itoh, K.Itoh, Reports of Research Institute for Ap-

plied Mechanics, Kyushu University No.134(1 - 3) (2008)
3) N.Kasuya, M.Yagi, K.Itoh and S.-I. Itoh, Phys. Plasma **15** 052302(2008)
4) Dan C. Sorescu. First principles calculation of the adsorption and diffusion of hydrogen on Fe(100) surface and in the bulk. Catalysis Today **105** 44 - 65(2005)v
5) T.Maruta, Kyushu-Univ. master thesis (2007)
6) K. Kamataki, Y. Nagashima, S. Shinohara, Y. Kawai, M. Yagi, K. Itoh and S. -I. Itoh, Journal of the Physical Society of Japan Vol. 76, No. 5, May, 2007, **054501**
7) P.H. Diamond et al., Nuclear Fusion, Vol. 41, No.8 (2001).
8) P.H.Diamond, S.-I.Itoh, K.Itoh and T.S.Hahm, Plasma Phys. Control. Fusion **47** 35 - 161 (2005)
9) K. Terasaka, S. Shinohara, Y. Nagashima, T. Yamada, M. Kawaguchi, T. Maruta, S. Inagaki, Y. Kawai, N. Kasuya, M. Yagi, A. Fujisawa, K. Itoh and S. -I. Itoh, Plasma Fusion Res. **2**,031(2007).
10) K. Terasaka, Kyushu-Univ. master thesis (2006)
11) S. Shinohara, Y. Nagashima, T. Yamada, M. Kawaguchi, K. Terasaka, T. Maruta, S. Inagaki, Y. Kawai, A. Fujisawa, M. Fukao, M. Ignatenko, M. Azumi, N. Kasuya, M. Yagi, K. Itoh, and S. -I. Itoh, in *Proc.28th Int.Conf. on Phenomena in Ionized Gases, Prague, Czech Republic*, 1P04-08, 354 (Institute of Plasma Physics ASCR, Prague,2007).
12) J. W. Connor: Plasma Phys. **19** (1977) 853
13) M. A. Lieberman and A. J. Lichtenberg: Principles of plasma discharges and material processing (Wiley, New Jersey, 2005) 2nd ed., p.727
14) D. Heifetz: in Physics of Plasma - Wall Interactions in Controlled Fusion, ed. D. E. Post and R. Behrisch (plenum, New York, 1986) p.695
15) J. M. Hammersley and D. C. Handscomb: Monte Carlo Methods (Wiley, New York, 1964)
16) E. E. Lewis and W. F. Miller: Computational Methods of Neutron Transport (Wiley, New York, 1984) p. 296.
17) M. H. Hughes and D. E. Post: J. Comput. Phys. **28** (1978) 43.
18) D. Heifetz, D. Post, M. Petravic, J. Weisheit, and G. Bateman: J. Comput. Phys. **46** (1982) 309.
19) G. J. M. Hagelaar, F. J. de Hoog, and G. M. W. Kroesen: Phys. Rev. E **62** (2000) 1452.
20) C. Schoroder, Ph.D. thesis, Ernst-Moritz-Arndt-University, Greifswald, 2003.